Understanding large plastic deformation of SiC nanowires at room temperature

J. WANG,[1,2,3,4] C. LU,[1,a)] Q. WANG,[3,b)] P. XIAO,[4] F. J. KE,[2,4] Y. L. BAI,[4] Y. G. SHEN,[5]

X. Z. LIAO,[6] and H. J. GAO[7]

[1]*Department of Mechanical Engineering, Curtin University - Perth, WA 6845, Australia*

[2]*School of Physics and Nuclear Energy Engineering, Beihang University - Beijing 100191, China*

[3]*School of Aeronautics Science and Engineering, Beihang University - Beijing 100191, China*

[4]*State Key Laboratory of Nonlinear Mechanics (LNM), Institute of Mechanics, Chinese Academy of Sciences - Beijing 100190, China*

[5]*Department of Manufacturing Engineering and Engineering Management (MEEM), City University of Hong Kong - Kowloon, Hong Kong, China*

[6]*School of Aerospace, Mechanical and Mechatronic Engineering, University of Sydney - Sydney, NSW 2006, Australia*

[7]*School of Engineering, Brown University - Providence, Rhode Island 02912, USA*

Abstract

Tensile behaviors of SiC [111] nanowires with various possible microstructures have been investigated by molecular dynamics simulations. The results show that the large plastic deformation in these nanowires is induced by the anti-parallel sliding of 3C-grains along an ultra-thin intergranular amorphous film parallel to the $(11\bar{1})$ plane and inclined at an angle of 19.47º with respect to the nanowire axis. The resulting large plastic deformation of SiC nanowires at room temperature is attributed to the stretching, breaking and re-forming of Si–C bonds in the intergranular amorphous film, which is also evident from the saw-tooth jumps in the stress-strain response.

PACS numbers: 31.15.xv, 62.25.-g, 62.23.Hj

a) E-mail: C.Lu@curtin.edu.au
b) E-mail: bhwangqi@sina.com

The mechanical properties of a material critically depend on its intrinsic structures at different length scales. Among these properties, strength and ductility are two most important ones that are often mutually exclusive and are determined by the physical nature of plastic deformation [1]. For example, materials like ceramics are strong but brittle; most metals, however, are just the opposite. An ideal material should be strong and also ductile. In most real applications, materials with high strength, such as ceramics, usually exhibit poor plasticity. One of the biggest challenges for material scientists is how to improve the deformation capacity of ceramic materials. According to the classical dislocation pile-up theory, the more difficult it is for dislocations to nucleate and slip, the stronger and more brittle a crystalline material becomes. However, this simplistic view breaks down in the case of nano-structured materials due to other deformation mechanisms [2-4]. To fully understand the mechanical response of nano-structured materials to external loading, many experimental studies have been carried out in the last decade. Novel mechanical behaviors have been observed due to their ultrafine grains and a rather high density of lattice defects in nano-structured materials. Several peculiar deformation mechanisms have been discovered in nano-structured metals such as rotational deformation, deformational twinning and grain boundary-mediated plasticity [5-7]. In contrast to studies on the super-strength of nano-structural metals, there have been relatively few efforts on understanding the properties of nano-structured ceramics. For example, SiC is intrinsically brittle at room-temperature, and the lack of ductility or plastic deformation has severely limited its applications. An interesting route to improve the deformation capacity of SiC and other ceramic materials has been the development of nano-structures [8].

Recently, significant advances have been made since SiC nanowires (NWs) were synthesized. For example, brittle to ductile transition and large strain plasticity in SiC NWs were detected with local stain reaching about 2%, which is in stark contrast to the typical strain level of 0.1–0.2% or even smaller of their bulk counterparts [9,10]. Almost at the same time, super-plasticity was found during uniaxial tensile loading of SiC NWs, with local strain exceeding 200%. The observed super-

plasticity was assumed to be due to dislocation nucleation, propagation and amorphization developed from cubic (3C) single crystal segments [11,12]. However, most analysis of tensile and bending deformation in SiC only revealed elastic behavior and brittle failure [13-16]. To address this apparent paradox, in this Letter, molecular dynamics simulations have been carried out to analyze the influence of various microstructures on the mechanical behaviors of SiC NWs, with focus on deformation mechanisms that result in the large plastic deformation behavior under uniaxial tensile loading.

The SiC NWs synthesized in laboratory usually consist of 3C-structured segments, stacking defects, twins, and an ultra-thin amorphous shell [17,18]. Moreover, an intergranular amorphous film (IAF) with thickness of 0.6 to 0.9 nm between grains was found as a result of aluminium added as sintering aid [19]. Since aluminium is always used to restrict the lateral growth in their synthesis, the IAF is most likely to exist in SiC NWs [20].

Considering that stacking defects occur on close packed planes like (111) or equivalent for the 3C-SiC, and the axis of an individual NW is along the [111] orientation, there are only two relative types of spatial configurations: stacking defects occurring at $(11\bar{1})$ and (111). The former forms an angle of 19.47^{o} with respect to the [111] orientation and the latter is vertical to the [111] orientation, as illustrated in Figs. 1(a) and (b). Stacking defects, twins and IAF can form at either of these angles, resulting in 6 possible spatial structures in SiC NWs, see Figs. 1(c) to (e).

To examine the contribution of each structure to the tensile behavior, 8 designed samples are adopted, including 3C-single crystal NW, amorphous shell NW, and the 6 possible structures mentioned above. Every sample has a round cross section with a diameter of 5 nm and an aspect ratio of length to diameter of about 6:1. To ensure traction-free boundary conditions, a vacuum region of 3 nm is attached on the outside of the lateral surface. Periodic boundary conditions are implemented along all the directions. The 3C-crystal segment is generated by an ordered sequence of three basic structure modules of tetrahedral bonding in SiC [21]. The stacking defects are

generated by randomly ordered sequences of these modules, while the twins are generated by anti-ordered sequences in comparison with that of the 3C-segment. The thickness of stacking defects or twins at an inclination angle of 19.47º is set to 2 nm, while the thickness of their perpendicular counterparts is 5 nm. The IAF is generated by filling amorphous film into a corresponding carved region in a prepared NW. The thickness of IAF is set to 0.75 nm, which lies in the middle of the measured range [19]. The thickness of the amorphous shell and the 3C-core are 1 and 1.5 nm, respectively. Dimensions of all the defects are designed by consulting the transmission electron microscope image of individual SiC NW, as shown in Fig. 1(f).

A quasi-static loading scheme at 300 K is employed to simulate and obtain the tensile deformation and mechanical properties of SiC NWs. The deformation increment along [111] is achieved by two steps. First, a modified isothermal-isobaric ensemble is used to stretch NWs with a strain rate of 0.001 ps^{-1} for 1 ps. This results in a nominal strain of 0.1% at each deformation increment [22]. Then, the axial strain is held and the wire is relaxed for 6 ps via a canonical ensemble [23]. The stress tensor is calculated by a modified virial formula [24]. More details of the numerical techniques were discussed in Ref. [25]. An interatomic potential consisting of two-body and three-body covalent interactions is used in molecular dynamics simulations with a time step of 2 fs by using the DL_POLY2.20 package [23,26]. All the samples are relaxed for 500 ps before stretching.

The typical stress-strain responses of SiC NWs containing stacking defects, twins and amorphous shell are shown in Fig. 2. In comparison with NWs containing stacking defects or amorphous shell, the 3C single crystal NW has the highest Young's modulus, strength and elongation of 289 GPa, 28.5 GPa and 10.7%, respectively. NWs with stacking defects at 19.47^{o} result in weaker modulus, strength and elongation than that of their perpendicular counterparts. Furthermore, the amorphous shell NW shows the lowest modulus and strength of 158 and 12.4 GPa, respectively. In a recent study, it was shown that the brittle to ductile transition could be triggered

by amorphous shell at temperature beyond 700 K [27]. Here, similar results were obtained at the room-temperature, and the brittle failure occurs at a strain of 9.5% without plastic behavior. It can be concluded that, therefore, none of these structures contributes to the large plastic deformation at room-temperature.

The IAF shows a significant impact on the tensile behavior, as shown in Fig. 3(a). The IAF–90º is not beneficial to plasticity (here, IAF–90° indicates the IAF being vertical or at an angle of 90º to the axis, and similar abbreviations are used hereafter). It induces brittle failure just at the location of IAF as soon as the strain reaches 4.5%; see inset in Fig. 3(a). This elongation is 53.6% smaller than the corresponding value of 9.7%, for NWs with stacking defects perpendicular to the axis (SD–90º). In contrast, IAF–19.47º shows qualitatively different behaviors. Specifically, Young's modulus drops by 7.3% from 275 to 255 GPa in comparison with that of NWs with SD–90º. The strength also decreases by 16.5% from 12.1 to 10.1 GPa. However, the plastic behavior occurs even before the tensile strength (i.e., point A in Fig. 3(a) with strain of 4.2%) is reached. Unloading from point A shows that a strain of 0.3% remains after the external force is completely removed. Unloading from a strain level of 4.3% (point B in Fig. 3(a)) leads to a residual strain of 1.6%, indicating the occurrence of large plastic deformation.

The plastic deformation is achieved through the anti-parallel sliding of two 3C-grains along $(11\bar{1})$ plane, as shown in Fig. 3(b). The tensile response shows saw-tooth jumps that result from stretching, breaking and re-forming of Si-C bonds in the IAF, see Figs. 3(c) to (e). Specifically, as strain increases from 8.5% to 9.6%, stretching of Si-C bonds in the IAF dominates the deformation (from C to D in Fig. 3(a)). As they reach their tensile limit, the stretched bonds break and lead to an abrupt stress drop until a new bond forms (from D to E in Fig. 3(a)). Thus, the anti-parallel sliding of the two 3C-grains result in repeated saw-tooth jumps. It is worth noting that the local unloading curve at point D is consistent with the corresponding loading curve at point C. That is, the stage of C to D of the saw-tooth origins from the elastic stretching of Si-C bonds in IAF. Furthermore, the

slope of the upswing portion of each saw-tooth (from C to D) is similar to that of the elastic regime of the stress-strain curve, indicating that the mechanical properties of SiC NWs are determined by the stretching limit of Si-C bonds in IAF. Repetition of this saw-tooth jumping behavior of stress-strain response produces a plastic elongation of 20.9% until brittle failure occurs in the right 3C-grain; see Fig. 3(f). The final elongation is 4.6 times of the corresponding value of 4.5% for the IAF–90º.

Among all possible structures, IAF–19.47º shows the lowest tensile strength. It is known that the mechanical behaviors of a material are closely related to its weaker section. The tensile behaviors of a wire are exclusively determined by the shearing deformation along the IAF–19.47º even if such a wire consists all the possible structures. Other structures have little contribution to the tensile strain because they are too strong to be deformed and their corresponding strengths cannot be reached.

A proper understanding of the large plastic deformation in SiC NWs can be given as follows. In the local region with an aspect ratio of 6:1, each IAF–19.47º shows a plastic elongation of 20.9%. In a cubic crystal, there are 4 close packed planes $(11\bar{1})$, $(1\bar{1}1)$, $(\bar{1}11)$ and (111). The former 3 form an angle of 19.47º with respect to the [111] orientation, while the latter is perpendicular to the axis. Therefore, there are 3 equivalent spatial possibilities for an IAF to form an inclination angle of 19.47º with respect to the [111] orientation and each of them has equal tendency to contribute to the plastic behaviour. However, the interaction among a higher density of IAFs and their effect on plastic deformation in SiC NWs is still an open challenge. Further, IAFs with the higher density and various spatial locations may converge to form a more complicated IAF network, known as amorphous grain boundaries, which may also contribute to local plasticity. Actually, the amorphous grain boundaries have already been proved to have significant impact on the plastic behavior of nano-structured SiC. There are extensive literatures focusing on the role of amorphous grain boundaries and the corresponding plastic behaviours have already been well analysed [28,29].

In summary, a comprehensive analysis via molecular dynamics simulations has been conducted to investigate the effects of possible microstructures on the tensile behavior of SiC NWs. The results show that only those structures with IAFs parallel to $(11\bar{1})$ and inclined at an angle of 19.47º with respect to the [111] orientation lead to large plastic deformation due to the anti-parallel sliding of 3C-grains along the IAFs. The resulting plastic deformation can be clearly seen through saw-tooth jumps in the stress-strain response, and its micro-mechanism is attributed to the stretching, breaking and re-forming of Si-C bonds in the IAF. It should be pointed out that this mechanism differs from the conventional plastic deformation in metals, which is usually associated with the generation and propagation of dislocations. The present study contributes to the understanding of large plastic deformation of nano-structured ceramics, especially for SiC NWs at room temperature. This work also provides guidance on the microstructural design for high-plastic ceramics with tailored mechanical properties.

This work was supported by the Australian Research Council (Grant No. DP0985450), the National Natural Science Foundation of China (Grant Nos. 10732090, 10932011, 11072014, 10972218 and 11021262) and the National Basic Research Program of China (2007CB814803). Computations were performed on computer clusters at the CNIC supercomputing Center, iVEC through the use of advanced computing resources located at iVEC@ARRC and parallel cluster acquired through the WCU program in the School of Mechanical and Aerospace Engineering at SNU.

References

[1] VALIEV R., *Nature (London)*, **419** 887 (2002).

[2] MEYERS M. A., MISHRA A., and BENSON D. J., *Prog. Mater. Sci*., **51** (2006) 427.

[3] LU C., MAI Y. W., and SHEN Y. G., *J. Mater. Sci.*, **41** (2006) 937.

[4] WANG Y. B. *et al*., *Adv. Mater.*, **23** (2011) 1356.

[5] MURAYAMA M. *et al.*, *Science*, **295** (2002) 2433.

[6] SHAN Z.W. *et al*, *Science*, **305** (2004) 654.

[7] LU L. *et al*., *Science*, **323** (2009) 607.

[8] KARCH J., BIRRINGER R., and GLEITER H., *Nature (London)*, **330** (1987) 556.

[9] HAN X. D. *et al.*, *J. Appl. Phys*., **98** (2005) 124307.

[10] HAN X. D. *et al.*, *Nano Lett.*, **7** (2007) 452.

[11] ZHANG Y. F. *et al.*, *Adv. Funct. Mater.*, **17** (2007) 3435.

[12] SZLUFARSKA I. *et al.*, *Appl. Phys. Lett*., **85** (2004) 378.

[13] ZHANG T. Y., LUO M., and CHAN W. K., *J. Appl. Phys*., **103** (2008) 104308.

[14] CHAN W. K., LUO M., and ZHANG T. Y., *Scr. Mater*., **59** (2008) 692.

[15] CHAN W. K., and ZHANG T. Y., *J. Appl. Phys*., **107** (2010) 023526.

[16] MAKEEV M. A., SRIVASTAVA D., and MENON M., *Phys. Rev. B*, **74** (2006) 165303.

[17] SHIM H. W., and HUANG H., *Appl. Phys. Lett*., **90** (2007) 083106.

[18] SHIM H. W., ZHANG Y., and HUANG H., *Appl. Phys. Lett*., **104** (2008) 063511.

[19] KIM Y. W., MITOMO M., and NISHIMURA T., *J. Am. Ceram. Soc*., **84** (2001) 2060.

[20] JING Q., LIANG P., and GUO X. Y., *J. Mater. Sci. Lett*., **22** (2003) 767.

[21] LINDEFELT U. *et al*., *Phys. Rev. B*, **67** (2003) 155204.

[22] MELCHIONNA S., CICCOTTI G., and HOLIAN B. L., *Mol. Phys*., **78** (1993) 533.

[23] SMITH W., YONG C. W., and RODGER P. M., *Mol. Simul*., **28**, (2002) 385.

[24] ZHOU M., *Proc. R. Soc. London*, **459** (2003) 2347.

[25] WANG J. *et al*., *Comput. Meth. Appl. Mech. Engrg*., **197** (2008) 3182.

[26] VASHISHTA P. *et al*., *J. Appl. Phys*., **101** (2007) 103515.

[27] WANG Z. G. *et al.*, *J. Phys. D: Appl. Phys*., **41** (2008) 155419.

[28] SZLUFARSKA I., NAKANO A., and VASHISHTA P., *Science*, **309** (2005) 911.

[29] MO Y. and SZLUFARSKA I., *Appl. Phys. Lett*., **90** (2007) 181926.

Figure captions

FIG. 1. (Color online) Illustrations of possible structures of SiC NWs. (a) 19.47^{o} stacking plane, (b) 90^{o} stacking plane, (c) schematic diagrams of stacking defects (SD) at inclination angles of 19.47^{o} and 90^{o} to the axis, (d) sketched map of twins (TW), (e) patterns of IAF and (f) an individual SiC NW adapted from Ref. [11]. Here, darker strips and lighter regions correspond to SD–90^{o} and 3C-segments, respectively. The thin black slashes in 3C-segments indicate defects with an inclination angle of 19.47^{o}, as illustrated in (c) to (e).

FIG. 2. (Color online) Stress-strain curves of SiC NWs with various structures. SD and TW denote stacking defects and twins, and angles indicate their relative spatial positions with respect to the axis. Amorphous shell is abbreviated to AS. Insets are typical patterns after the brittle failure of NWs.

FIG. 3. (Color online) (a) Stress-strain curves in the cases of IAF–90^{o} and IAF–19.47^{o}, respectively. Inset is the failure pattern of IAF–90^{o}. (b) Anti-parallel sliding of two grains along the IAF, where arrows indicate sliding directions. (c), (d) and (e) demonstrate the micro-mechanisms of a saw-tooth jump in the stress-strain response, in which stretching and re-forming of bonds are highlighted by circles and box, respectively. (f) A snapshot of IAF–19.47^{o} after failure.

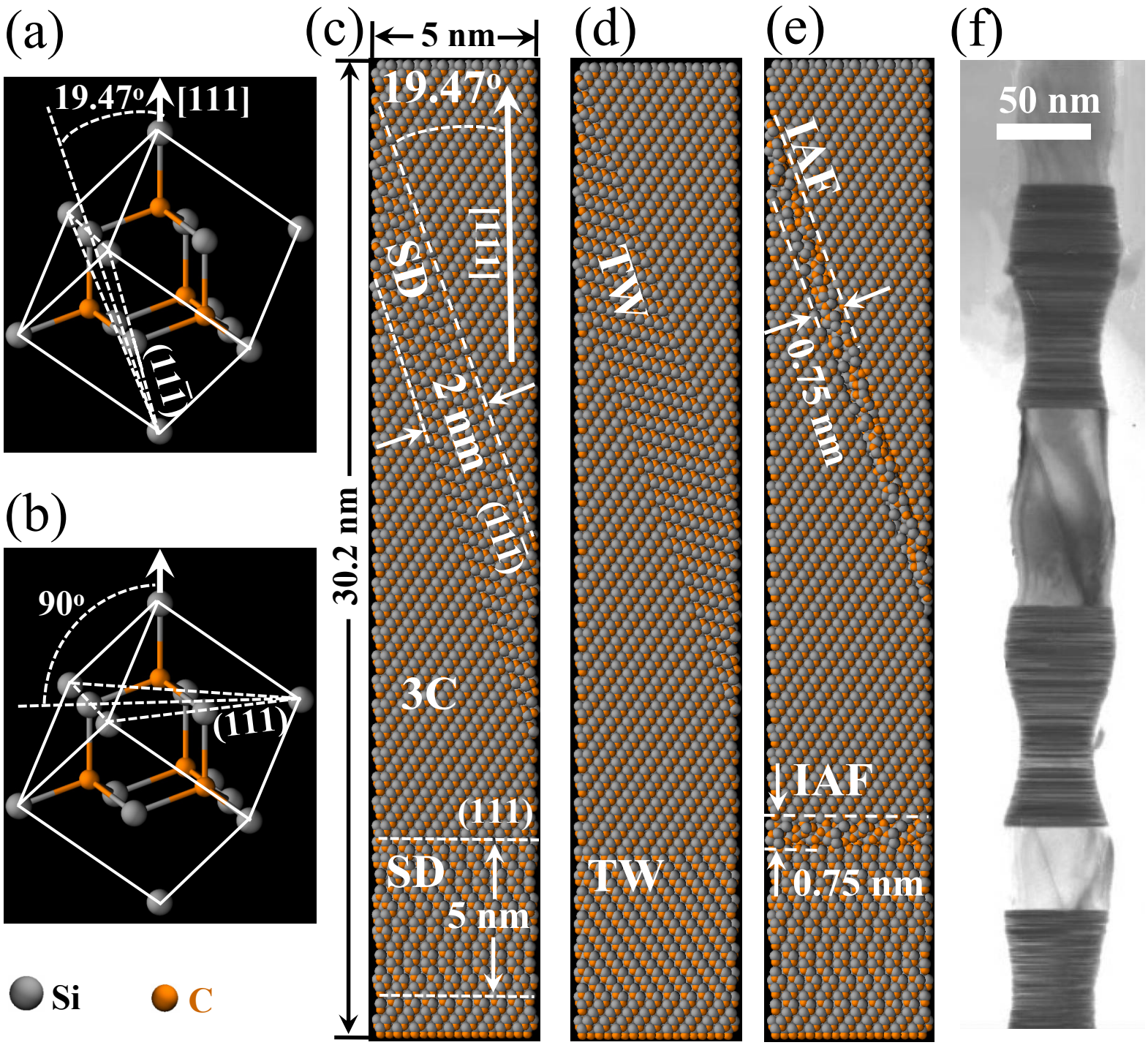
(a)
19.47°
[111]
(11$\bar{1}$)
(b)
90°
(111)
Si
C
(c)
5 nm
19.47°
[111]
SD
2 nm
(11$\bar{1}$)
30.2 nm
3C
(111)
SD
5 nm
(d)
TW
TW
(e)
IAF
0.75 nm
IAF
0.75 nm
(f)
50 nm

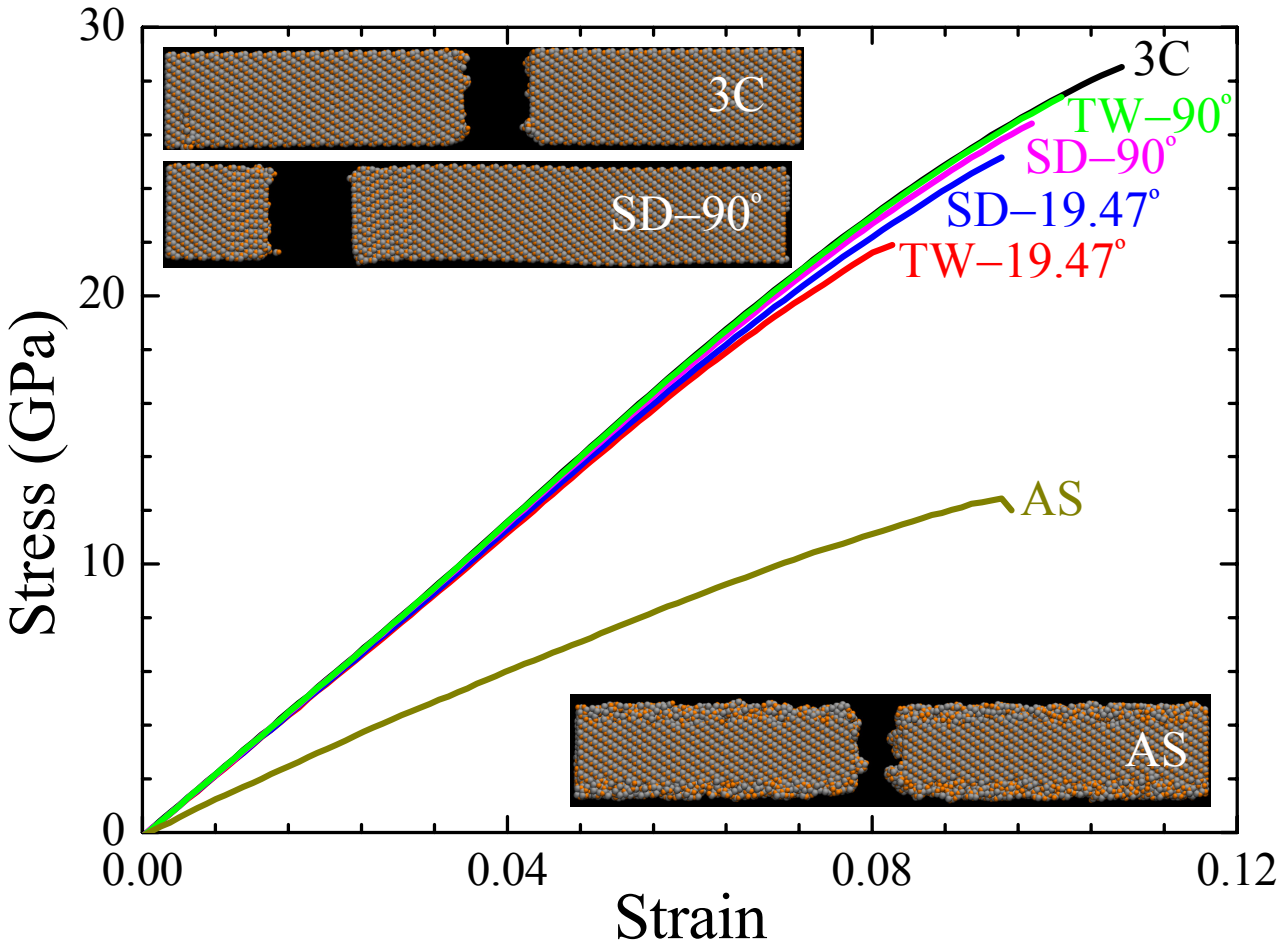
30
20
10
0
0.00
0.04
0.08
0.12
Stress (GPa)
Strain
3C
TW–90°
SD–90°
SD–19.47°
TW–19.47°
AS
3C
SD–90°
AS

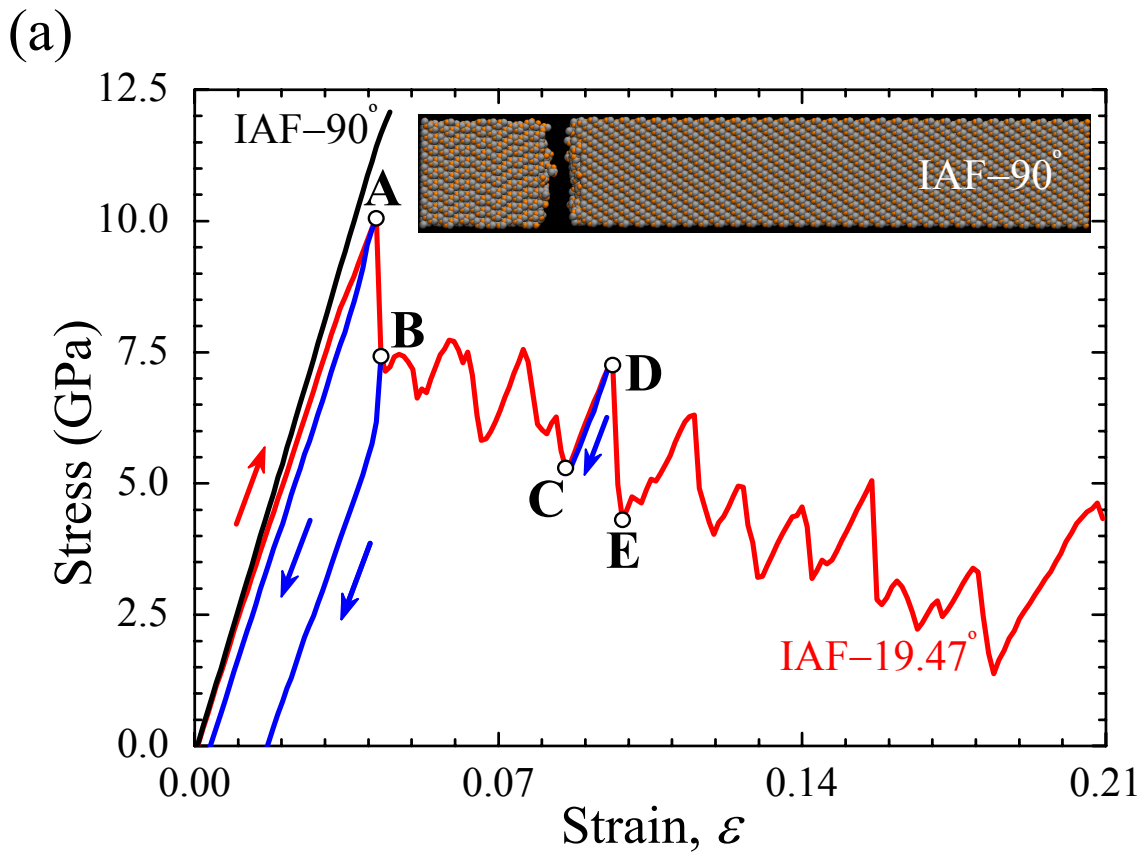
(a)
12.5
10.0
7.5
5.0
2.5
0.0
Stress (GPa)
0.00
0.07
0.14
0.21
Strain, ε
IAF–90°
IAF–90°
A
B
C
D
E
IAF–19.47°

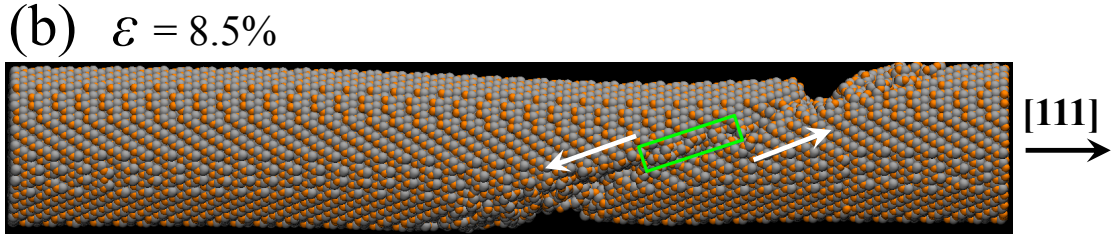
(b) ε = 8.5%
[111]

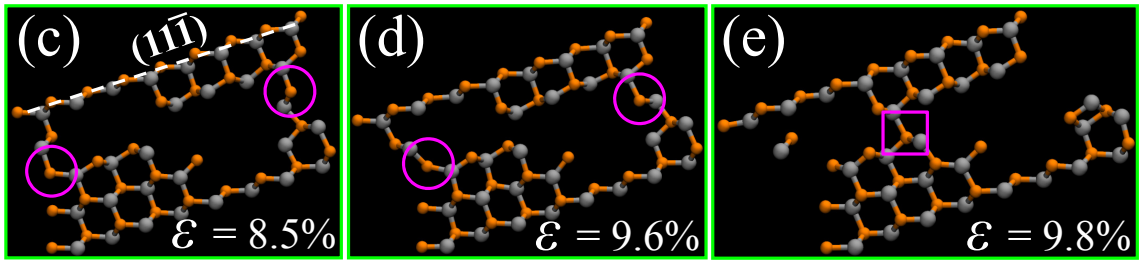
(c)
(11$\bar{1}$)
ε = 8.5%
(d)
ε = 9.6%
(e)
ε = 9.8%

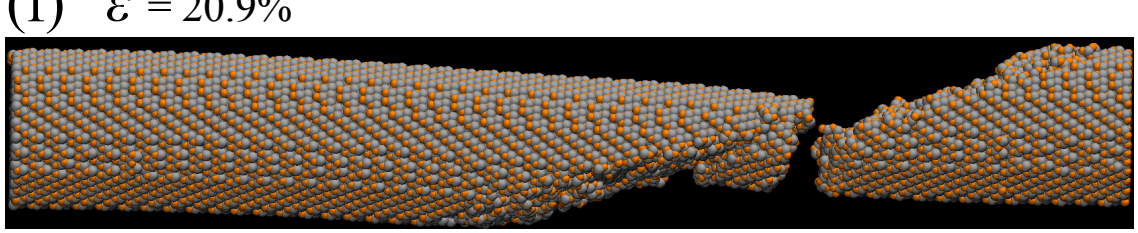
(f) ε = 20.9%